

Comments nubs.acs.org/cm

# Reply to "A Comparison of the Stochastic and Deterministic Approaches in a Nucleation-Growth Type Model of Nanoparticle Formation"



Cite This: https://doi.org/10.1021/acs.chemmater.1c01690



ACCESS

Metrics & More



Article Recommendations

# I. INTRODUCTION

In a recent comment, I addressed challenges with the Finke-Watzky (F-W) model purported to describe nanoparticle nucleation and growth. In that comment I noted similar challenges applied to the related Szabó and Lente's model (SL).<sup>2</sup> A response to that comment was simultaneously published by Finke, Watzky, and Whitehead (FWW).3 And in the preceding comment, Szabó and Lente (SL) provide an additional response. The purpose of my initial comment was to highlight that (1) the dimensionality or particle size must be included in any description of particle growth and (2) to describe the consecutive processes of nucleation and growth it is necessary to use serial, and not parallel, mathematical functions. As such, it generally is not possible to extract details of the independent nucleation and growth processes from a single average measurement of the transformation of reactant to product with time.

SL interpreted my comment highlighting the need to recognize that nucleation and growth are independent, serial processes as a challenge to the well-known reality that a large number of stochastic processes generally can be described by a deterministic model. Herein, as described in Section II of this reply, it is critical to differentiate the relationship between stochastic and deterministic processes from the deconvolution of distinct processes, such as nucleation and growth, which may, or may not be separated in time. It should be noted that the M-KJMA model, 5,6 used in my prior comment is also a deterministic model of stochastic processes. (A further note of clarification: I have never advocated that the M-KJMA model is a preferred model to describe nanoparticle growth. In my initial comment I specifically stated that this "analysis in no way seeks to imply that the M-KJMA model is the accurate model for nanoparticle growth. ... Nevertheless, the M-KJMA analysis demonstrates clearly that any model of actual particle growth must include particle size, nucleation frequency, and initial nucleation time parameters."1)

In their comment, SL further address whether stochastic vs deterministic treatment of nucleation and growth models impact the particle size distribution (PSD) of nanoparticles. While their simulations confirm that stochastic vs deterministic models do not account for any substantial variation in nanoparticle PSD's, their models fail to reproduce realistic PSD's. In Section III of this reply, SL's simulations are compared to an alternative simulation with a stoichiometrically precise ensemble-nucleation/monolayer-shell-growth model

(EN/MSG), evaluated with respect to experimental data from the seminal report of Turkevich et al. This EN/MSG simulation reaffirms it is the consecutive nature of nucleation and growth, rather than stochastic vs deterministic effects, that control a nanoparticle's PSD.

However, based on comments from certain reviewers and published responses to my initial comment, 3,8 before addressing these two points from the SL comment, it is evident that some clarification language is necessary.

My use of the terms serial and parallel specifically refers to mathematical functions to describe distinct processes. No concept of "serial nucleation" has been introduced. To be clear, the consecutive nature of particle nucleation and subsequent growth must be described by serial mathematical functions. Nucleation creates the initiating nanocrystalline lattice out of a disordered ensemble of precursors. Growth propagates an already established lattice. In a many particle system, the consecutive (serial) processes of nucleation and growth may (or may not) be concurrent. If the processes of nucleation and growth are concurrent, a parallel mathematical function may approximate both processes. However, as demonstrated in my original comment, accurate deconvolution of the actual independent serial functions from an approximate parallel function is generally not possible.

Second, comments from reviewers highlight the need to precisely define what is meant by nucleation, with two reviewers suggesting that nanoparticle nucleation may begin with the condensation of only 2-3 monomers. Nucleation is important with respect to the condensation of liquid droplets from the gas phase, the formation of amorphous or crystalline species from solution, the formation of crystalline species from melts or glasses, etc. While each rightly is described as nucleation, they are likely mechanistically distinct. In my previous comment and this reply, I am specifically referring to the nucleation of crystalline nanoparticles from solution. It is impossible to distinguish whether the assemblage of only 2-3monomers is a nucleus of a liquid, glass or crystal, effectively a nucleation uncertainty principle. What distinguishes a crystal

Received: May 17, 2021



from other states of matter is the existence of a regular periodic lattice. The first Brillion zone of a lattice harmonic oscillator, equivalent to twice the lattice constant, establishes the minimum size of a lattice, and thus is also the limiting minimum size of a nanocrystalline nucleus.

# II. STOCHASTIC/DETERMINISTIC VS SEPARATING CONSECUTIVE PROCESSES

In their comment, SL state, "The present comment has been written to address a point that was brought up by both Martin and Finke: the stochastic nature of single nucleation events must be considered in really quantitative models. The problem in the background is that classical (deterministic) chemical kinetics works with concentrations as continuous functions of time at the macroscopic or ensemble level, whereas in reality matter is composed of particles and all molecular events actually occur atomistically or molecularly between discrete particles."

It is not a point of debate that increasing the number of stochastic events provides results that can be better and better approximated by a deterministic function. This can readily be demonstrated with a simple comparison of a normal distribution of 10, 100, 1000, etc. stochastic events to the Gaussian distribution function. While the specific event distribution changes with each simulation, increasing the number of stochastic events per simulation clearly produces a distribution that more closely corresponds to the deterministic Gaussian distribution function.

As correctly noted by SL, the same principles apply to modeling chemical kinetic processes, which are related to discrete atomic, molecular, monolayer, particle, etc. events at the microscopic level. Since these processes often occur in many-particle systems, actual reaction measurements generally can be modeled as continuous deterministic functions.

Importantly with respect to nanoparticle formation, both nucleation and growth, in their microscopic limits, are stochastic processes. However, they are chemically and physically distinct processes that may occur concurrently or may be separated in time. Furthermore, nucleation, while being a stochastic collection of singular events, <sup>10,11</sup> happens only once for each primary particle. Particle growth, only occurring after the particle has nucleated, also can be considered a stochastic process that involves the addition of monomers to the growing particle, or the aggregation of previously formed primary particles. Unlike nucleation, particle growth involves many repeated addition steps to the same particle, continuing until either the monomer is depleted or until another reactive step becomes competitive.

Deconvolution of the consecutive processes of nucleation and growth is a major challenge in developing models of nanoparticle formation. Unlike the distinct stochastic processes of nucleation and growth, which may be independently modeled with deterministic functions, the convolution of consecutive processes generally cannot be accurately modeled by a parallel deterministic function such as is done in both the SL and the F–W models.

However, experimentally the ability to separately control nucleation and growth has been exploited to achieve significant control over particle sizes and shapes. Interestingly, in the Turkevich et al. example of gold nanoparticle formation, they demonstrated that only about 5% of the chloroauric acid is consumed by the time that nucleation is complete. Furthermore, they and others demonstrated that, under certain conditions, no additional nucleation occurs

when preformed gold nanoparticle nuclei are added to the growth medium.

To demonstrate the challenges of modeling such consecutive processes with parallel functions, in my previous comment I demonstrated the impact of varying nucleation time and frequency under a constant growth condition on the overall progress of particle formation. Using simple simulations with five particles to model burst vs linear-continuous nucleation (see JDM-Figure 2) or nucleation with four distinct induction times (see JDM-Figure 3), it was demonstrated that systems with more nuclei generated early in the reaction exhibit the fastest apparent reaction rates. Applying the F-W two-step (or SL) deterministic nucleation and growth model to those simulations demonstrates their inability to differentiate distinct nucleation and growth profiles. A change to only the nucleation rate in the simulation, for example, manifests as a change to both the modeled nucleation and growth rate constants.

The impact of the independence of nucleation and growth is further highlighted by an in-depth consideration of the simulations reported in the preceding SL comment. In their comment, SL-Figure 1, "the results for the time dependence of the scaled concentration of the monomeric units from five stochastic simulation runs and the corresponding deterministic curve at the fixed values of  $k_n/k_g = 10^{-6}$  and  $n = 10^{6}$ " are presented. Their deterministic curve is described as eq 1 (SL-eq 3)

$$[M] = \frac{[M]_0 k_g e^{-k_g [M]_0 t}}{2k_n + (k_g - 2k_n) e^{-k_g [M]_0 t}}$$
(1)

where  $[M]_0 = n_0/N_A/V$  ( $n_0$  is the number of monomers,  $N_A$  is Avogadro's number, and V is the volume),  $k_g$  is a growth rate constant, and  $k_n$  is a nucleation rate constant. Notably, their stochastic simulations demonstrate a significant distribution of reaction rates for a constant set of input parameters. The rate distributions for their simulations are further represented by their plots of half-lives of the various simulation runs, presented in SL-Figure 3 and their supplemental SL-Figures S3 and S4.

In Figure 1, the SL deterministic curve is reproduced using eq 1 (large black circles) and superimposed on the solid black circles of the reproduced original figure. Notably, fitting each of the simulated runs to eq 1 returns distinct  $k_n/k_g$  ratios. For the fastest simulation, Run 4,  $k_n/k_g = 2.00 \times 10^{-6}$  (blue circles), and for the slowest simulation, Run 1,  $k_n/k_g = 1.75 \times 10^{-7}$  (red circles).

However, there is nothing about the stochastic simulation that should change the  $k_n/k_g$  ratio. Instead, the randomization of nucleation in their stochastic simulation statistically results in initial nucleation occurring at earlier or later times for each simulation run. To address this time deviation from the stochastic mean,  $t_s$  can be introduced into eq 1 to yield eq 2.

$$[\mathbf{M}] = \frac{[\mathbf{M}]_0 k_g e^{-k_g [\mathbf{M}]_0 (t - t_s)}}{2k_n + (k_g - 2k_n) e^{-k_g [\mathbf{M}]_0 (t - t_s)}}$$
(2)

If  $t_s = 0$ , then the initial nucleation of that stochastic simulation is equivalent to that expected from the deterministic model, i.e., nucleation begins at the first time step past t = 0, and the number of nuclei increases monotonically thereafter until the reactant begins to be depleted. If, however, a stochastic scenario yields a larger than average number of nuclei in the initial time steps, then the reaction will appear to

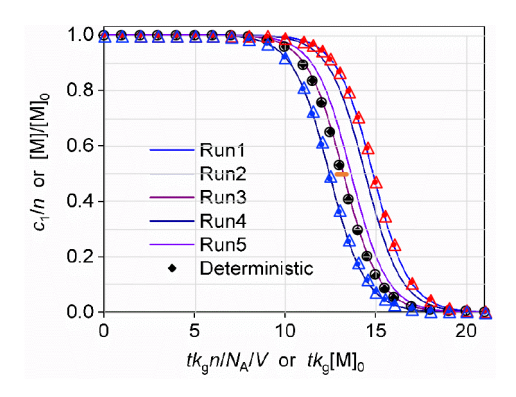


**Figure 1.** SL's stochastic simulations reproduced from SL-Figure 1 of their comment; open black circles represent the deterministic eq 1 with  $n=10^6$  and  $k_n/k_g=10^{-6}$ . Deterministic calculations based on  $k_n/k_g$  ratios fit to eq 1 (solid red and blue circles) and with  $t_s$  fit to eq 2 using the simulation's  $k_n/k_g=10^{-6}$  ratio (open red and blue triangles). The short orange line represents the spread of  $t_{1/2}n/N_A/V$  from SL-Figure S3 describing simulations with  $n=10^8$  and  $k_n/k_g=10^{-6}$ . Data from ref 4. Copyright 2021 The Authors under https://creativecommons.org/licenses/by/4.0/deed.ast.

proceed faster than the deterministic model, which is reflected as a negative value for  $t_s$ . By contrast, if a stochastic scenario exhibits no nucleation in the first several time steps, then the reaction will appear to proceed slower than predicted by the deterministic model, reflected by a positive value for  $t_s$ .

Using eq 2, one finds that each of SL's simulations can be completely described using their simulation parameter of  $k_n/k_g$  =  $10^{-6}$ , but with the initial stochastic nucleation times of  $t_s$  = -0.65 for Run 4 (open blue triangles) and  $t_s$  = 1.76 for Run 1 (open red triangles).

In their comment, SL-Figure 3 and supplemental SL-Figures S3 and S4 present the distribution of half-lives observed for 100 simulations for each of three sets of n and  $k_n/k_g$  input parameters. They do not present such data for the other 95 simulations for the input parameters  $n=10^6$  and  $k_n/k_g=10^{-6}$  for SL-Figure 1 discussed above. SL-Figure S3 does provide data for conditions  $n=10^8$  and  $k_n/k_g=10^{-6}$ , for which  $\Delta t_{1/2}n/N_A/V$  is about 0.46, represented as the short orange line in Figure 2. That distribution is notably narrower than  $\Delta t_{1/2}n/N_A/V$  of 2.5 for the reported five simulation runs in Figure 2; the total distribution for the full set of 100 simulations is likely substantially larger than observed for the limited set of five simulations reported. Similarly,  $\Delta t_{1/2}n/N_A/V$  is about 1.1 for the data reported in SL-Figure 3 with  $n=10^8$  and  $k_n/k_g=10^{-7}$  and about 8.8 for the data reported in SL-Figure S4 with  $n=10^8$ 

 $10^8$  and  $k_n/k_g=10^{-8}$ . While the median stochastic and corresponding deterministic  $t_{1/2}n/N_A/V$  value is determined by the  $k_n/k_g$  ratio, the distribution of  $t_{1/2}n/N_A/V$  is correlated with the magnitude of n with respect to the  $k_n/k_g$  ratio. For a constant  $k_n/k_g$  ratio, increasing the concentration of monomer particles narrows the distribution of  $t_{1/2}n/N_A/V$ , consistent with a greater probability that, under higher concentrations, the stochastic  $t_s$  will go to 0, equivalent to the deterministic model. Note additionally that the reported  $t_{1/2}n/N_A/V$  values are normally distributed about the stochastic mean, a consequence of the random number generator used to define the stochastic nucleation probabilities.

Thus, a deeper analysis of the more complex simulations reported in the SL comment<sup>4</sup> reinforce one of the conclusions made in my original comment, i.e., that the initial time and frequency of nucleation must be considered when evaluating the overall rate of nanoparticle formation.<sup>1</sup> It further demonstrates that separation of the consecutive processes of nucleation and growth has a physical/chemical basis and is not an artifact of stochastic vs deterministic models.

# III. NUCLEATION AND PARTICLE SIZE DISTRIBUTION

In their comment, SL also consider whether stochastic or deterministic models result in any differences in the resultant particle size distribution (PSD).<sup>4</sup> Herein, they consider the size of the particle to be proportional to the cube root of the number of monomeric units in it. For the stochastic simulations, the size of each of the simulated particles is determined from its number of monomers. Their deterministic model of particle size is described by eq 3 (SL-eq 4).

$$\langle r \rangle = r_0 \sqrt[3]{ -k_n + \frac{2k_g k_n (k_g - 2k_n) e^{-k_g [M]_0 t}}{2(k_g - 2k_n)(1 - e^{-k_g [M]_0 t})} \ln \left( \frac{k_g}{2k_n + (k_g - 2k_n) e^{-k_g [M]_0 t}} \right)}$$
(3)

SL note that while the deterministic model demonstrates a monotonic increase in average particle size with time, the stochastic frequency of nucleation can result in short periods of a decrease in the average particle size because of the very small size of each new nucleus.<sup>4</sup> It would be extremely difficult to experimentally measure and, thus, confirm (or not) whether such phenomena are real. Nevertheless, both of their deterministic and stochastic models yield essentially equivalent PSDs.

However, the final PSD in nanoparticle syntheses is a measurable quantity that can provide insight as to whether a model may provide a reasonable representation of actual nucleation and growth processes. Classical models of

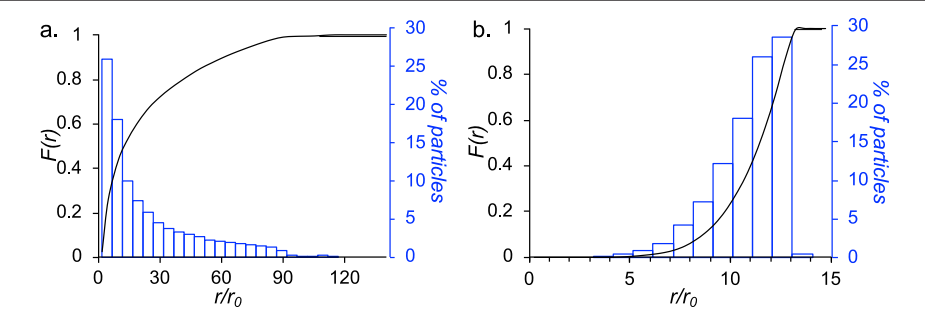


**Figure 2.** Reproduced SL figures of final PSD for (a) the SL-particle size dependent,  $SL_{psd}$  (SL-Figure 4), and (b) SL-particle size independent,  $SL_{psi}$  (SL-Figure 6), models. Here these data are converted to PSD histograms with bin sizes of  $5 r/r_0$  in (a) and  $1 r/r_0$  in (b) (blue secondary axis). SL figures from ref 4. Copyright 2021 The Authors under https://creativecommons.org/licenses/by/4.0/deed.ast.

nucleation and growth suggest that the distribution of particle size is strongly dependent on the distribution in the time of nucleus formation. As stated by Turkevich et al., Particles formed early in the nucleation process begin to grow immediately so that in the final sol the particles that first form and hence have the longest time to grow, attain the largest size. Nuclei which form later attain smaller and smaller sizes corresponding to shorter and shorter growing times. It must be noted that this assumption does not consider nonclassical aggregative growth, nor does it consider possible effects of surface-ligand termination on particle growth.

Herein, the SL comment presents a comparison of the final PSD for their stochastic and deterministic models. Figure 2 reproduces two of their figures, with their data converted to PSD histograms for comparison to traditional literature reports of nanoparticle size distribution. SL-Figure 4 (reproduced in Figure 2a) presents the normalized final PSD for simulations based on the primary SL model, eq 3. In that model, the rate of particle growth scales with the size of the particle (described here as the particle size dependent model,  $SL_{psd}$ ). The input parameters were  $n=10^8$  and  $k_n/k_g=10^{-6}$ . SL-Figure 6 (reproduced as Figure 2b) presents the final PSD for a second SL model that presumes the rate of particle growth is independent of particle size effects (here described as  $SL_{psi}$ ). The input parameters were  $n=10^7$  and  $k_n/k_g=5\times 10^{-8}$ .

As expected, because of the continuous nucleation in the SL models (and F–W models), a continuous PSD from zero to the maximum particle size is observed. It is not intuitively clear why the largest number of nuclei in the  $SL_{psd}$  model are very small (Figure 2a). These data suggest that for this  $SL_{psd}$  model nucleation becomes fast with respect to growth at later stages of the reaction. By contrast, the  $SL_{psi}$  model indicates that the greatest number of nuclei are formed at the initial stage of the reaction when the monomer concentration is the highest (Figure 2b). In both models, the nuclei that emerge first grow the largest.

The final PSD generated with both SL models is not characteristic of most experimentally observed PSDs, which exhibit both lower and upper bounds to the PSD. As exemplars, consider the particle size histograms in references 7, 9, and 13.

Using population balance models, Perala and Kumar previously demonstrated that the F-W two-step particle formation mechanism with the presumption of continuous nucleation does not reproduce experimental PSDs.<sup>20</sup> Furthermore, in two recent manuscripts, Finke et al. evaluated PSDs with respect to multiple models with continuous nucleation. They conclude that, "the 2-step mechanism ... is incapable of reproducing the more information rich PSD." Finke et al. were only able to approximately model experimental PSDs using their continuous nucleation hypothesis with an assumption that small particles grow faster than large particles so that monodispersity is achieved by "allowing the smaller particles to catch up to the more slowly growing larger particles."<sup>22</sup> However, such a requirement is inconsistent with historical observations that "if the diffusion [of monomer] is the ratedetermining quantity, then the rate of change of diameter is inversely proportional to the diameter; while if the process is limited by the surface reaction, then the rate of change of dimeter with time is independent of the particle diameter." Under the relevant conditions of nanoparticle syntheses being modeled, particle growth is substantially slower than the rate of diffusion, indicating mechanistic models should be based on surface reactions, not diffusion. For aggregative growth, i.e., independent of monomer concentration, the particle growth rate is smaller for larger particles.<sup>23,24</sup>

Furthermore, the difference between the SL modeled PSDs and the experimental PSDs clearly is not a function of stochastic vs deterministic modeling. As demonstrated in SL-Figures 4 and 6, the stochastic and deterministic approaches yield essentially equivalent results, but neither is at all reflective of the experimental PSDs. Instead, as demonstrated below, the distinction between their modeled and experimental PSDs results from the failure to treat nucleation as an independent process that must be deconvoluted from particle growth.

While many aspects of nucleation remain unresolved, classical nucleation theory (CNT) suggests there is a critical size required for a nucleus to form. The critical nucleus size from CNT is considered to be a function of surface energy. However, many recent reports suggest nonclassical nucleation by the formation of amorphous prenucleation clusters. Whether CNT or non-CNT, nucleation apparently involves the assembly of some minimum number of monomers, which define a minimum limit to the PSD.

As noted in the introduction, the minimum size of a crystal lattice, and thus presumably the minimum size crystal nuclei, must be at least greater than two times the lattice constants. Literature reports suggest the sizes of the nanoparticle or crystal nuclei are typically between 10 and 1000 monomers but up to 40 nm for the nucleation of the protein apoferritin.<sup>25</sup> Turkevich et al. estimate the size of a gold particle nucleus to be 30-40 Å in diameter (based on a close packing of a sphere model this size nucleus would consist of 900-2000 gold atoms, equivalent to 6 to 8 times the  $d_{(100)}$  of an fcc unit cell). More recent TEM experiments where HAuCl<sub>4</sub> is reduced by an electron beam demonstrate initial gold nanoparticle nuclei of between 10 and 38 Å in diameter (approximately between 55 and 2,000 atoms, equivalent to 2 to 8 times the  $d_{(100)}$  of an fcc unit cell).<sup>29</sup> And recently Ramamoorthy et al. showed that 40 Å prenucleation clusters of gold monomers collapse to 20 Å nanocrystal nuclei (approximately 300 atoms, equivalent to 4 times  $d_{(100)}$  of an fcc unit cell).<sup>28</sup>

If, however, the minimum of a final PSD is larger than the size of the initial nuclei, as is commonly observed, then particle growth must have continued well past the completion of nuclei formation. This is clearly observed in the Turkevich et al. systems demonstrating completion of nucleation before more than 5% of the monomer is consumed.<sup>7</sup>

The maximum in the PSD is fundamentally limited by the amount of material (# of monomers) with respect to the number of nucleated particles. For a given amount of material, fewer nuclei result in larger particles, and more nuclei result in smaller particles. This effect is seen in the sodium citrate concentration and monomer dilution experiments by Turkevich et al. (Figures 5, 6, 16, and 17 of that manuscript) for which higher amounts of nucleation at high sodium citrate concentration or low overall dilution result in the smallest maximum particle size.<sup>7</sup> It also has been demonstrated that the addition of artificially introduced nuclei (seeds) can suppress the formation of new nuclei, allowing growth to continue well past the end of nucleation. 7,12,13,17 Note, if the SL (and FW) continuous nucleation model prevailed, then double maxima in the PSD would be observed when seeds are introduced into reaction systems with additional monomer.

Thus, experimentally the overall final PSD appears to be determined by a serial combination of independent nucleation

and growth functions. It is possible to test this proposed model with a relatively simple simulation which (a) defines an initial nucleus size, (b) reproduces the experimentally reported nucleation rates, and (c) applies a chemically and geometrically realistic growth model.

- (a) Consistent with Turkevich et al.'s experimental report of the likely nucleus size being between 30 Å to 40 Å, an initial nucleus size was set to be 923 Au atoms based on a cuboctahedron of close packed gold atoms (~30 Å in diameter;  $6 \times d_{(100)}$  and  $4 \times d_{(111)}$ ). Mechanistically, this ensemble-nucleation model reflects organization of the ensemble of monomers making up an amorphous prenucleation cluster into a nascent crystal lattice in a manner similar to crystal nucleation from a melt.
- (b) The experimental nucleation rate data for the sodium citrate and acetone dicarboxylic acid reduction of gold nanoparticles yielding the PSDs reported in ref 7 were digitized from the original manuscript (Figure 17 Standard and Figure 13, respectively) and normalized to 100%, Figure 3.

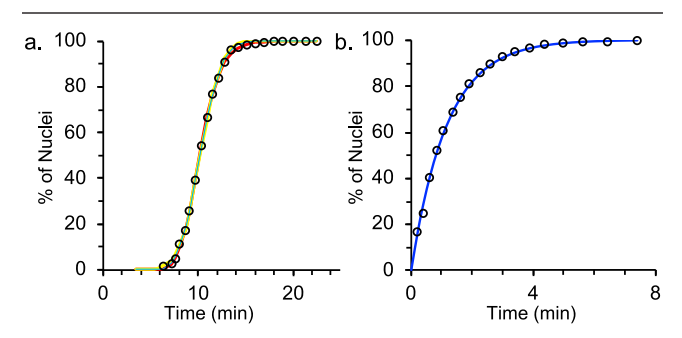


Figure 3. Nucleation Frequency Functions describing the nucleation rate for the (a) standard sodium citrate and (b) acetone dicarboxilic reduction of HAuCl<sub>4</sub>. Functions are compared to experimental data (black circles) reported by Turkevich et al. Sodium citrate data are equally represented by the autocatalytic-type function eq 4 (thick red line), a normal distribution eq 5 (medium yellow line), and the empirical function eq 6 (thin blue line). Acetone dicarboxilc acid data are well represented by the empirical function eq 7 (blue line).

Multiple functions can equivalently describe the sigmoidal profile of the sodium citrate nucleation. Turkevich et al. suggested the sigmoidal profile to be a result of an autocatalytic reaction. However, as one reviewer pointed out, no autocatalytic  $A+B\rightarrow 2B$  reaction describes the conversion of citrate to acetone dicarboxylate. Nevertheless, an autocatalytic-like, two rate constant function eq 4 (thick red line of Figure 3) can model the sigmoidal nucleation frequency vs time.

$$N_t = N_f \times \left( 1 - \frac{k_1 + k_2}{k_2 + k_1 \exp((k_1 + k_2)(t - t_0))} \right)$$
 (4)

where  $N_t$  is the number of nuclei produced at time t,  $N_f$  is the final number of nuclei, here set to 100 to generate 0 to 100% of nuclei,  $k_1 = 0.0483$  and  $k_2 = 0.818$ , and  $t_0$  is an induction time of 6.81 min.

Alternatively, the nucleation frequency data can be equivalently fit by the normal time distribution, eq 5,

$$N_t = N_f \times \left( \frac{1}{\sigma \sqrt{2\pi^2}} \exp\left( -0.5 \left( \frac{t - \mu}{\sigma} \right)^2 \right) \right)$$
 (5)

for  $N_f = 100$  nuclei with  $\mu = 10.558$  min and  $\sigma = 1.803$  (medium yellow line in Figure 3) or with an empirical stretched exponential function, eq 6 (thin blue line in Figure 3)

$$N_t = N_f \times (1 - \exp(-k(t - t_0)^3))$$
 (6)

where  $k = 6.55 \times 10^{-3} \text{ min}^{-3}$  is an empirical rate constant and  $t_0$  is an induction time of 5.51 min.

Acetone dicarboxylic acid was determined to be a direct nucleating agent and, thus, exhibits no induction time for nucleation. Here, the time dependent nucleation can be modeled with a simple empirical exponential function, eq 7, where  $k = 0.851 \text{ min}^{-1}$ .

$$N_t = N_f \times (1 - \exp(-kt)) \tag{7}$$

No claims are made here as to whether any of these expressions yield parameters with mechanistic significance; instead, they simply model the experimentally observed time dependent nucleation frequency. Equation 4, with three fitting parameters, gives a slightly superior fit to the number of nuclei (std = 0.74) than that of the two-parameter eqs 5 (std = 1.13) and 6 (std = 1.03) for the sodium citrate-based nucleation. Because eqs 4-6 yield equivalent results, for the simulations herein, eq 6, with fewer fitting parameters, was used to model the nucleation frequency. The acetone dicarboxylic acid nucleation data is well fit with the single fitting parameter of eq 7 (std = 1.09).

(c) A growth model was generated based on monolayer-shell growth of a cuboctahedron with close packed gold atoms. This model is consistent with experimental reports of particle diameters increasing at a common rate irrespective of the particle size. Both historic and modern experimental studies demonstrate that reactive crystal/nanoparticle growth from solution exhibits fast growth across a given monolayer, with substantially slower growth into a next monolayer. This generally results in the completion of growth of a given monolayer before the next begins. Thus, monolayer shell addition can be considered the rate limiting step of particle growth.

Such monolayer shell growth can be stoichiometrically defined, but not in the simplistic manner of the SL model 2M  $\rightarrow$  C<sub>2</sub>, C<sub>i</sub> + M  $\rightarrow$  C<sub>i+1</sub><sup>2</sup> (or the F–W model A  $\rightarrow$  B, A + B  $\rightarrow$ 2B<sup>3</sup>) elementary steps. As a particle grows, only the sites at the surface of the particle can be reactive toward subsequent monomer addition; thus, the particle's core [C] (or core [B]) should not appear in any rate expressions. This means the growth rate should scale with number of surface sites, not the total number of incorporated monomers, described by SL as i. 4 Thus, the SL-equation for  $i \ge 2$ ,  $r_{g,i} = ik_g[M][C_i]$ , cannot define realistic particle growth. Notably, in SL-eq 3 they include the term i only to describe  $[C_i]$ ; it does not appear in their equation to describe the consumption of monomer, [M], nor in SL-eq 4 describing the average size of the nanoparticles. <sup>4</sup> A surface area dependent function, r(j), dependent on the particle size j, was incorporated into some of the F-W population balance models. 21,22 The surface area dependence is present as a "words only" statement about "autocatalytic surface growth" in earlier F-W models for which any surface area function is absent from the actual rate laws.<sup>32</sup> The lack of a needed surface area function in the rate law was the primary basis for my previous comment.

To understand the stoichiometry of monolayer particle growth, consider the model described in Figure 4, where the

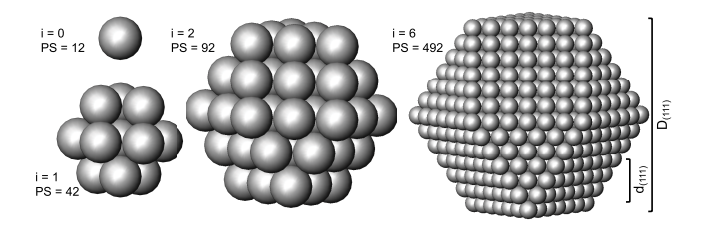


**Figure 4.** Growth of a cuboctahedral particle of cubic close packed monomers. Scale bars show the height of the body diagonal of one unit cell,  $d_{(111)}$ , compared to the i = 6 particle diameter,  $D_{(111)}$ .

index i is used to count the number of monomer shells added to the nuclear core. Here, a single atom/molecule monomer is placed at the nuclear core at i=0. Based on cubic close packing of spherical monomers, 12 monomers can be added in the first monomer shell i=1, for a particle total  $P_m=13$  monomers. This suggests that the initial core monomer can be considered to have 12 particle reactive sites, PS=12. The next monomer shell, i=2, adds 42 monomers such that  $P_m=55$ . But this also means that shell i=1 has PS=42.

The number of PS for a particle with i monomer shells for such a cuboctahedron of cubic close packed spheres is precisely defined by eq 8.

$$PS_i = 10(i+1)^2 + 2 (8)$$

The total number of monomers in the cuboctahedral particle with i monomer shells,  $P_{ij}$  is precisely defined by eq 9.

$$P_i = \frac{10}{3}i^3 + 5i^2 + \frac{11}{3}i + 1 \tag{9}$$

The diameter of the growing particle scales with the height of the (111) and (100) layers and the radius of the monomer,  $r_0$ , described by eq 10.

$$D_{(111)} = \left(\frac{4\sqrt{6}}{3}i + 2\right)r_0$$

$$D_{(100)} = (2\sqrt{2}i + 2)r_0$$
(10)

The assumption of the constant rate of particle growth further suggests that  $\mathrm{d}i/\mathrm{d}t$  is a particle growth rate constant  $k_g$ . This of course assumes conditions of a monomer activity of 1, possibly a reality for melt crystallization, but not for particle growth from solution as modeled herein. Assuming a

bimolecular-type reaction between monomers and the available  $PS_n$  which is first order in monomer concentration, then

$$\frac{\mathbf{d}_i}{\mathbf{d}_t} = k_g \frac{M_t}{M_0} \tag{11}$$

where  $M_0$  is the original number of monomers in the system and  $M_t = M_0 - \sum P_i$ , where  $\sum P_i$  is the total number of monomers that have been incorporated into all growing particles.

Based on the above ensemble-nucleation/monolayer-shell growth assumptions, EN/MSG simulations were constructed using an initial 30 Å nucleus size of 923 monomers corresponding to  $i_{nuc} = 6$  as described in (a), nucleation profiles as described in (b) for samples of 100 nuclei, and the growth model as described in (c). Thus, for each of the 100 particles, at  $t = t_n$  for that particle,  $i_t = i_{nuc} = 6$ . At  $t > t_n$  for each particle,

$$i_t = i_{(t-\delta t)} + k_g \frac{(M_0 - \sum P_i)}{M_0} (\delta t)$$
 (12)

At each time step,  $\delta t$ ,  $P_i$  is calculated using eq 9 for each of the particles that is nucleated. The values of  $P_i$  for all particles are summed to determine  $M_t$  for the subsequent time step. These numbers of monomer shell data are then converted to the respective particle sizes using eq 10 based on an average of  $D_{(111)}$  and  $D_{(100)}$  with  $r_0 = 1.439$  Å for gold.

Simulations were conducted to compare this nucleation and growth model to the experimental nucleation rate and PSD data reported by Turkevich et al. for the sodium citrate and acetone dicarboxylic acid reduction of HAuCl4. The average particle size from each histogram (Figures 4 and 14 of the original manuscript) was calculated for the experimentally reported PSD from each reductant (193 and 202 Å, respectively) to determine the value for  $M_0 = 3 \times 10^7$  to simulate the nucleation and growth of 100 nanoparticles ( $M_0 = 2.8 \times 10^7$  and  $3.2 \times 10^7$ , respectively). The time of nucleation for each of the 100 particles was determined using the stretched exponential eq 6, fit to the experimental nucleation data for the sodium citrate, and eq 7 for the acetone dicarboxylic acid reduction of HAuCl<sub>4</sub>.

The results of the simulation corresponding to the sodium citrate reduction are given in Figure 5. This simple simulation remarkably reproduces the experimentally reported final PSD<sup>7</sup> when  $k_g = 0.05 \text{ MLS} \cdot \text{s}^{-1}$  (MLS = monolayer shells) This optimal growth rate coupled with the experimentally determined nucleation rate also shows that only 5% of the

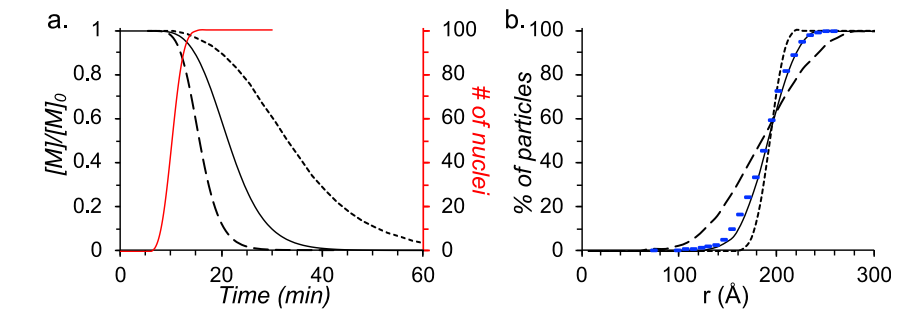


Figure 5. (a) Time-dependent nucleation of 100 Au particles (red line) based on the eq 6 fit to the experimental nucleation data. The consumption of monomer  $[M]/[M]_0$  was simulated according to eq 12 with  $k_g = 0.025$  MLS·s<sup>-1</sup> (short dashed line), 0.05 MLS·s<sup>-1</sup> (solid black line), and 0.10 MLS·s<sup>-1</sup> (long dashed line). (b) Final PSDs from each of these three simulation conditions (black lines) compared with the experimentally reported PSD (blue dashes).

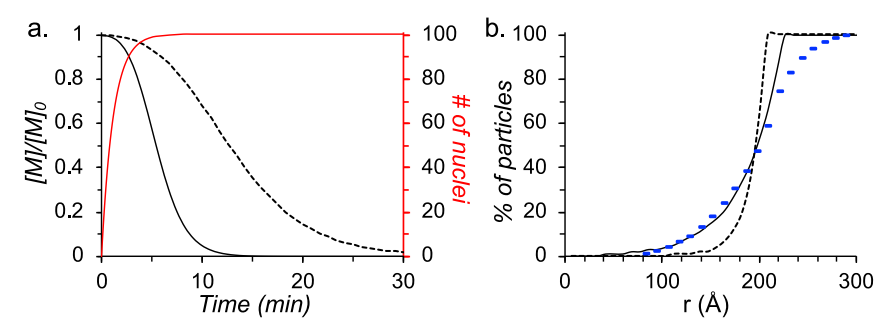


Figure 6. (a) Time-dependent nucleation of 100 Au particles (red line) based on the eq 7 fit to experimental nucleation data. The consumption of monomer  $[M]/[M]_0$  was simulated according to eq 12 with 0.125  $MLS \cdot s^{-1}$  (solid black line) and 0.050  $MLS \cdot s^{-1}$  (dashed line). (b) Final PSDs from each simulation condition (black lines) are compared with the experimentally reported PSD (blue dashes).

monomer has been consumed when nucleation is 95% complete, consistent with the experimental report. Doubling the growth rate constant to  $k_{\rm g}=0.10~{\rm MLS\cdot s^{-1}}$  (long dashed lines in Figure 5) creates a scenario where nucleation and growth overlap in time to a greater extent, which correspondingly results in a broader PSD. By contrast, cutting the growth rate in half to  $k_{\rm g}=0.025~{\rm MLS\cdot s^{-1}}$  further separates in time the nucleation and growth processes. Such conditions result in a substantially narrower PSD (short dashed lines in Figure 5).

Different behavior is observed for the EN/MSG simulations based on the distinct nucleation function reported for the acetone dicarboxylic acid reduction of HAuCl<sub>4</sub>.<sup>7</sup> The results of simulations with the acetone dicarboxylic acid nucleation frequency and two distinct growth rates,  $k_g = 0.125 \text{ MLS} \cdot \text{s}^{-1}$ and 0.050 MLS·s<sup>-1</sup>, are given in Figure 6. Because no induction time is reported under these conditions, both nucleation and growth initiate immediately. Note here that the sigmoidal onset of monomer consumption is a consequence of the geometric requirements of 3D particle growth, not a nucleation induction time. Again it is observed that the PSD is substantially broader with a faster growth rate relative to nucleation, because these conditions exhibit the most concurrent nucleation and growth. At  $k_g = 0.125 \text{ MLS} \cdot \text{s}^{-1}$ 18% of the monomer is consumed when 95% of the nuclei have formed, whereas when  $k_g = 0.05 \text{ s}^{-1}$  only 4% of the monomer is consumed when 95% of the nuclei have formed. However, as clearly seen in Figure 6b this nucleation and growth model does not accurately reflect the observed final PSD.

The simulated scenario with  $k_g = 0.125 \text{ MLS} \cdot \text{s}^{-2}$  remarkably matches the PSD for the smallest 50% of particles, likely reflecting the particles that nucleated at the latest times. However, the strict ensemble-nucleation and growth by the monomer attachment model predicts that the burst-type nucleation profile observed for acetone dicarboxylic acid reduction of HAuCl<sub>4</sub> should exhibit a sharp upper bound to the PSD, observed in the simulation but not in the experimental measurements. By contrast, growth by particle aggregation will shift and broaden the PSD toward larger size. The fusion of two medium size particles creates one large particle with no change in the amount of monomer consumed. Such aggregative growth was demonstrated for silver nanoparticle formation via the sodium borohydride reduction of silver perchlorate<sup>23</sup> and by electron beam reduction of silver nitrate.<sup>24</sup> Reaction conditions that support growth by monomer attachment generally yield isotropic particle shapes

whereas reaction conditions that support aggregative growth lead to particles with oval or more irregular shapes.<sup>7,12,33</sup>

#### IV. CONCLUSIONS

Clearly, understanding the consecutive nature of nucleation and growth as opposed to a stochastic vs deterministic treatment is important to decipher the mechanism(s) for nanoparticle growth. While models treating nucleation and growth as a parallel mathematical function, such as those proposed by SL and F–W, may reproduce the sigmoidal characteristics observed for monomer consumption, they do not accurately describe nanoparticle nucleation and growth. This is evident by the failure to reproduce experimental PSDs. Both my simulations and the above further analysis of SL's simulations demonstrate that the particle nucleation times must be explicitly addressed to model nanoparticle formation.

Because nanoparticles are ensemble systems, simple  $C_i + M \rightarrow C_{i+1}$  stoichiometric descriptions of nanoparticle formation reaction mechanisms cannot be defined. While M may be a well-defined monomer,  $C_i$  changes in character with each added monomer as a nanocrystalline lattice is built up. Furthermore, monomers internal to the particle cannot participate in its growth. However, the precise stoichiometry of particle growth can be defined based on the cubic close packing of the monomers, as was done herein for the growth of cuboctahedral particles. This precise particle stoichiometry is the basis for a concentration dependent monolayer-shell growth model that initiates from a nucleus of a finite size.

The model presented here does not resolve the complex chemistry required for the formation of an initial nucleus. Nucleation may occur by any number of possible mechanisms (e.g., Turkevich et al.'s organizer mechanism, LaMer's nucleation by a critical condensation of monomers from locally supersaturated domains, 34,35 a condensed matter-type nucleation of amorphous prenucleation clusters, 26-28 or countless other models). Nevertheless, the precise mechanism of nucleation is not critical to demonstrate the importance of using a nucleation frequency function that is independent from growth to describe nanoparticle formation. Clearly, modeling of the final PSD is achieved using the presented EN/MSG consecutive nucleation and growth model, which uses experimentally determined nucleation rates and a stoichiometrically precise particle growth model, which is superior to that achieved using the SL model which treats nucleation and growth with a parallel mathematical function.

James D. Martin 6 orcid.org/0000-0001-7414-2683

# AUTHOR INFORMATION

Complete contact information is available at: https://pubs.acs.org/10.1021/acs.chemmater.1c01690

#### Notes

The author declares no competing financial interest.

# ACKNOWLEDGMENTS

This work was supported by National Science Foundation via Contracts DMR-1709370 and DMR-1950984.

#### REFERENCES

- (1) Martin, J. D. Particle Size is a Primary Determinant for Sigmoidal Kinetics of Nanoparticle Formation: A "Disproof" of the Finke-Watzki (F-W) Nanoparticle Nucleation and Growth Mechanism. *Chem. Mater.* **2020**, 32, 3651–3656.
- (2) Szabó, R.; Lente, G. Full Analytical Solution of a Nucleation-Growth Type Kinetic Model of Nanoparticle Formation. *J. Math. Chem.* **2019**, *57*, 616–631.
- (3) Finke, R. G.; Watzky, M. A.; Whitehead, C. B. Response to "Particle Size is a Primary Determinant for Sigmoidal Kinetics of Nanoparticle Formation: A "Disproof" of the Finke-Watzki (F-W) Nanoparticle Nucleation and Growth Mechanism. *Chem. Mater.* **2020**, *32*, 3657–3672.
- (4) Szabó, R.; Lente, G. A. Comparison of the Stochastic and Deterministic Approaches in a Nucleation—Growth Type Model of Nanoparticle Formation. *Chem. Mater.* **2021**, DOI: 10.1021/acs.chemmater.0c04688.
- (5) Dill, E. D.; Josey, A. A.; Folmer, J. C. W.; Hou, F.; Martin, J. D. Experimental determination of the crystallization phase boundary velocity in the halozeotype CZX-1. *Chem. Mater.* **2013**, 25, 3932–3940.
- (6) Dill, E. D.; Folmer, J. C. W.; Martin, J. D. Simulating crystallization to elucidate the parameter space in the KJMA condensed phase transformation model. *Chem. Mater.* **2013**, *25*, 3941–3951.
- (7) Turkevich, J.; Stevenson, P. C.; Hillier, J. A Study of the Nucleation and Growth Processes in the Synthesis of Colloidal Gold. *Discuss. Faraday Soc.* **1951**, *11*, 55–75.
- (8) Whitehead, C. B.; Özkar, S.; Finke, R. G. LaMer's 1950 model of particle formation: a review and critical analysis of its classical nucleation and fluctuation theory basis, of competing models and mechanisms for phase-changes and particle formation, and then of its application to silver halide, semiconductor, metal and metal-oxide nanoparticles. *Mater. Adv.* 2021, 2, 186–235.
- (9) Whitehead, C. B.; Finke, R. G. Nucleation Kinetics and Molecular Mechanism in Transition-Metal Nanoparticle Formation: The intriguing Informative Case of a Bimetallic Precursor, {[(1,5-COD)Ir<sup>I</sup>·HPO<sub>4</sub>]<sub>2</sub>}<sup>2-</sup>. Chem. Mater. 2019, 31, 2848–2862.
- (10) Izmailov, A. F.; Myerson, A. S.; Arnold, S. A statistical understanding of nucleation. *I. Cryst. Growth* **1999**, 196, 234–242.
- (11) Maggioni, G. M.; Mazzotti, M. Stochasticity in Primary Nucleation: Measuring and Modeling Detection Times. *Cryst. Growth Des.* **2017**, *17*, 3625–3635.
- (12) Bastús, N. G.; Comenge, J.; Puntes, V. Kinetically Controlled Seeded Growth Synthesis of Citrate-Stabilized Gold Nanoparticles of up to 200 nm: Size Focusing versus Ostwald Ripening. *Langmuir* **2011**, *27*, 11098–11105.
- (13) Jana, N. R.; Gearheart, L.; Murphy, C. J. Seeding Growth for Size Control of 5–40 nm Dameter Gold Nanoparticles. *Langmuir* **2001**, *17*, 6782–6786.
- (14) Lohse, S. E.; Murphy, C. J. The Quest for Shape Control: a History of Gold Nanorod Synthesis. *Chem. Mater.* **2013**, *25*, 1250–1261.
- (15) Aizenberg, J. Crystallization in Patterns: A Bio-Inspired Approach. *Adv. Mater.* **2004**, *16*, 1295–1302.
- (16) Rimer, J. D.; An, Z.; Zhu, Z.; Lee, M. H.; Goldfarb, D. S.; Wesson, J. A.; Ward, M. D. Crystal Growth Inhibitors for the

- prevention of l-Cystine Kidney Stones Through Molecular Design. *Science* **2010**, 330, 337–341.
- (17) Wuithschick, M.; Birnbaum, A.; Witte, S.; Sztucki, M.; Vainio, U.; Pinna, N.; Rademann, K.; Emmerling, F.; Kraehnert, R.; Polte, J. Turkevich in New Robes: Key Questions Answered for the Most Common Gold Nanoparticle Synthesis. *ACS Nano* **2015**, *9*, 7052–7071
- (18) Deyoreo, J. J.; Gilbert, P. U. P. A; Sommerdijk, N. A. J. M; Penn, R. L.; Whitelam, S.; Joester, D.; Zhang, H.; Rimer, J. D.; Navrotsky, A.; Banfield, J. F.; Wallace, A. F.; Michel, F. M.; Meldrum, F. C.; Cölfen, H.; Dove, P. M. Crystallization by particle attachment in synthetic, biogenic, and geologic environments. *Science* **2015**, *349*, aaa6760.
- (19) Mozaffari, S.; Li, W.; Thompson, C.; Ivanov, S.; Seifert, S.; Lee, B.; Kovarik, L.; Karim, A. M. Colloidal nanoparticle size control: experimental and kinetic modeling investigation of the ligand-metal binding role in controlling the nucleation and growth kinetics. *Nanoscale* **2017**, *9*, 13772–13785.
- (20) Perala, S. R. K; Kumar, S. On the Two-Step Mechanism for Synthesis of Transition-Metal Nanoparticles. *Langmuir* **2014**, *30*, 12703–12711.
- (21) Handwerk, D. R.; Shipman, P. D.; Whitehead, C. B.; Özkar, S.; Finke, R. G. Mechanism-Enabled Population Balance Modeling of Particle Formation en Route to Particle Average Size and Size Distribution Understanding and Control. *J. Am. Chem. Soc.* **2019**, *141*, 15827–15839.
- (22) Handwerk, D. R.; Shipman, P. D.; Whitehead, C. B.; Özkar, S.; Finke, R. G. Particle Size Distributions via Mechanism-Enabled Population Balance Modeling. *J. Phys. Chem. C* **2020**, *124*, 4852–4880.
- (23) Van Hyning, D. L.; Klemperer, W. G.; Zukoski, C. F. Silver Nanoparticle Formation: Predictions and Verification of the Aggregative Growth Model. *Langmuir* **2001**, *17*, 3128–3135.
- (24) Woehl, T. J.; Park, C.; Evans, J. E.; Arslan, I.; Ristenpart, W. D.; Browning, N. D. Direct Observation of Aggregative Nanoparticle Growth: Kinetic Modeling of the Size Distribution and Growth Rate. *Nano Lett.* **2014**, *14*, 373–378.
- (25) Karthika, S.; Radhakrishnan, T. K.; Kalaichelvi, P. A Review of Classical and Nonclassical Nucleation Theories. *Cryst. Growth Des.* **2016**, *16*, 6663–6681.
- (26) Bewernitz, M. A.; Gebauer, D.; Long, J.; Cölfen, H.; Gower, L. B. A metastable liquid precursor phase of calcium carbonate and its interactions with polyaaspartate. *Faraday Discuss.* **2012**, *159*, 291–312.
- (27) Gebauer, D.; Wolf, S. E. Designing Solid Materials from Their Solute State: A Shift in Paradigms toward a Holistic Approach in Functional Materials Chemistry. J. Am. Chem. Soc. 2019, 141, 4490–4504.
- (28) Ramamoorthy, R. K.; Yildirim, E.; Barba, E.; Roblin, P.; Vargas, J. A.; Lacroix, L.-M.; Rodriguez-Ruiz, I.; Decorse, P.; Petkov, V.; Teychené; Viau, G. The role of pre-nucleation clusters in the crystallization of gold nanoparticles. *Nanoscale* **2020**, *12*, 16173—16188.
- (29) Loh, N. D.; Sen, S.; Bosman, M.; Tan, S. F.; Zhong, J.; Nijhuis, C. A.; Král, P.; Matsudaira, P.; Mirsaidov, U. Multistep nucleation of nanocrystals in aqueous solution. *Nat. Chem.* **2017**, *9*, 77–82.
- (30) Volmer, M. Zum Problem des Kristallwachstumus. Z. Phys. Chem. 1922, 102U, 267–275.
- (31) Maliakkal, C. B.; Mårtensson, E. K.; Tornberg, M. U.; Jacobsson, D.; Persson, A. R.; Johansson, J.; Wallenberg, L. R.; Dick, K. A. Independent Control of Nucleation and Layer Growth in Nanowires. *ACS Nano* **2020**, *14*, 3868–3875.
- (32) Watzky, M. A.; Finke, R. G. Transition Metal Nanocluster Formation Kinetic and Mechanistic Studies. A New Mechanism When Hydrogen Is the Reductant: Slow, Continuous Nucleation and Fast Autocatalytic Surface Growth. *J. Am. Chem. Soc.* **1997**, *119*, 10382–10400.

- (33) Frens, G. Controlled Nucleation for the Regulation of the Particle Size in Monodisperse Gold Suspensions. *Nature, Phys. Sci.* 1973, 241, 20–22.
- (34) LaMer, V. K.; Kenyon, A. S. Kinetics of the formation of monodispersed sulfur sols from thiosulfate and acid. *J. Colloid Sci.* **1947**, *2*, 257–264.
- (35) LaMer, V. K.; Dinegar, R. H. Theory, Production and Mechanism of Formation of Monodispersed Hydrosols. *J. Am. Chem. Soc.* **1950**, 72, 4847–4854.

1